THE JOURNAL OF PHYSICAL CHEMISTRY Letters

Letter

pubs.acs.org/JPCL

Ab Initio Study of $BiFeO_3$: Thermodynamic Stability Conditions

E. Heifets,*[,†] E. A. Kotomin,*[,†,‡] A. A. Bagaturyants,[§,∥] and J. Maier[†]

[†]Max Planck Institute for Solid State Research, 70569 Stuttgart, Germany

[‡]Institute for Solid State Physics, University of Latvia, Riga, LV-1586, Latvia

[§]Photochemistry Center, Russian Academy of Sciences, Moscow, Russia, 119991

[∥]National Research Nuclear University MEPhI (Moscow Engineering Physics Institute), Moscow, Russia, 115409

ABSTRACT: $BiFeO_3$ is investigated intensively, mainly as a multiferroic material. In this paper, the state-of-the-art ab initio hybrid functional approach with atomic basis sets was employed for a study of the stability range of $BiFeO_3$ with respect to its decomposition into binary oxides and elementary metals, as a function of temperature and oxygen partial pressure. The calculated atomic and electronic structure of $BiFeO_3$ was compared with previous LDA+U calculations using plane-wave basis sets. Based on performed calculations, the phase diagram was constructed, which allows us to predict the stability region of stoichiometric $BiFeO_3$.

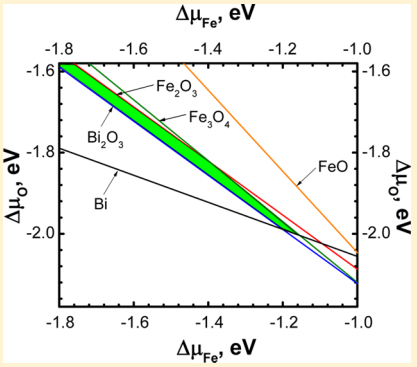

$BiFeO_3$ (BFO) perovskite-type material has attracted great attention due to its multiferroic and other important properties.[1−3] Recently, related perovskite solid solutions $(Bi_{1-x}Sr_xFeO_{3-\delta}$ and $Bi_{1-x}Sr_xFe_{1-y}Co_yO_{3-\delta})$[4−13] were also proposed as cathodes for solid oxide fuel cells (SOFCs) operating at intermediate (800−1000 K) temperatures. Understanding of thermodynamic stability conditions for BFO is important and represents the first step for future investigations of intrinsic defects, surface structures, surface chemical reactions (e.g., oxygen reduction reaction), the formation of various solid solutions such as the cathode materials mentioned above, and their possible structures and stability. The data on BFO stability could provide important information on conditions for manufacturing this and related materials.

A number of theoretical studies on BFO have been performed within the past few years. Among them, the relative stability of various charged defects was considered in refs 14 and 15, whereas the formation enthalpy of defect-free BFO was analyzed in ref 16 in order to determine parameters for optimal BFO thin film growth. In these simulations, the local density approximation (LDA) with the on-site Hubbard correction for interatomic Coulomb interactions (LDA+U) was applied. In such materials, the effective one-center Coulomb interaction parameter U_{eff} usually depends on the oxidation state of the transition or *f*-metals, and the use of a single Hubbard U parameter for different oxidation states is not well justified. This method deficiency could be overcome by using hybrid exchange-correlation functionals, where the exchange functional is mixed with precise nonlocal Fock's exchange. The calculations employing the hybrid functionals usually give much better descriptions of the electronic structure (band gaps) of nonmetallic materials, independently of the oxidation state of transition metals.[17−19]

We report here the results of ab initio calculations of BFO and possible products of its decomposition—binary oxides—bismuth oxide Bi_2O_3 and Fe oxides (FeO, Fe_2O_3, and Fe_3O_4) in various phases, in order to determine the range of possible chemical potentials for all three elements involved (Bi, Fe and O) at which BFO can exist. These ab initio structure calculations were used further in the thermodynamic stability analysis of BFO allowing us to identify its stability region.

Ab initio calculations were performed with CRYSTAL09 computer code.[20] This code uses Gaussian-type basis functions centered at atomic nuclei, to expand one-electron orbitals. The B3PW hybrid functional[20−25] was employed in all ab initio calculations in this study. It includes a "hybrid" of nonlocal exact Fock's exchange, gradient-corrected (generalized gradient approximation (GGA)), and local (local-density approximation) exchange potentials combined with the GGA correlation potential of Perdew and Wang. The presence of Fe in the considered materials suggests strong electron correlation effects. The use of a hybrid functional allows for a more appropriate treatment of interactions between electrons, greatly reducing the self-interaction error of standard density functionals.

Series of Coulomb and exchange integrals were truncated with overlap thresholds[26] of 10^{-8}, 10^{-8}, 10^{-8}, 10^{-8}, and 10^{-16}. The Monkhorst−Pack grid for integration over the Brillouin zone in the reciprocal space was chosen such that the distance

Received: May 22, 2015
Accepted: July 4, 2015

DOI: 10.1021/acs.jpclett.5b01071
J. Phys. Chem. Lett. 2015, 6, 2847−2851

Table 1. Lattice Parameters and Energy Differences between Two Phases of $BiFeO_3$[a]

			Space group		Lattice parameters				
Phase	Obtained from	Magnetic order	label	number	a=b, Å	c, Å	γ, °	Z	ΔE, meV/molecule
FE	Expt.[29]	AFM	R3C	161	5.581	13.876	120°	2	
	Opt.	FM			5.614	14.101	120°	2	208
	Opt.	AFM:G			5.596	14.000	120°	2	0
cubic	Opt.	FM	$Pm\bar{3}m$	221	7.854	7.854	90°	8	1280
distorted cubic	Opt.	AFM:A			7.859	7.815	90°	8	1166
	Opt.	AFM:C			7.824	7.860	90.0°	8	1057
	Opt.	AFM:G			7.829	7.829	90°	8	963

[a]Angles $\alpha = \beta = 90°$ in the unit cells of all crystal structures considered in this table.

Table 2. Optimized and Experimental Atomic Positions (Fractional Units) within Conventional Unit Cell in FE Structure of $BiFeO_3$

atom	symmetry position	calculated			expt.[29]		
Bi	a	0.0000	0.0000	0.0000	0.0000	0.0000	0.0000
Fe	a	0.0000	0.0000	0.2237	0.0000	0.0000	0.2208
O	b	0.4378	0.0169	0.9547	0.4452	0.0176	0.9520

Table 3. Standard Gibbs Energies of Formation (ΔG^0_f) and the Formation Energies (ΔE_f, equals ΔG_f at 0 K) of Bi and Fe Oxides and $BiFeO_3$[a]

material	phase	magnetic order		ΔE_f, eV	ΔG^0_f, eV	error, %
FeO	cubic	AFM:[111]	expt.[31]	−2.88	−2.61	
			all-e	−3.05	−2.77	6.5
Fe_2O_3	α-phase	AFM	expt.[31]	−8.50	−7.68	
			all-e	−8.26	−7.45	−3.1
Fe_3O_4	cubic	FiM:↑↑ ↓↓↓↓	expt.[31]	−11.63	−10.55	
	rhobohedral		all-e	−11.48	−10.39	−1.4
Bi_2O_3	α-phase		expt.[31]	−5.97	−5.15	
$BiFeO_3$	FE	AFM:G	expt.[32]	−7.97(−0.71)	−7.15 (−0.71)	
			all-e	−7.17 (−0.05)	−6.35 (−0.05)	−11.2

[a]Arrows in the case of Fe_3O_4 describe magnetic configuration of the ground ferrimagnetic state, where the atomic spins of two iron ions in tetragonal sites (denoted by two first arrows) have opposite direction than the atomic spins of four iron ions in octahedral sites (last four arrows). Values for $BiFeO_3$ in brackets are formation energies and Gibbs energies with respect to the formation of $BiFeO_3$ from Bi_2O_3 and Fe_2O_3. The errors represent deviations of calculated formation Gibbs energies from experimental values.

between the neighboring points of the net is no more than ~0.18 $Å^{-1}$ for all the considered materials and employed unit cells. The self-consistent procedure in all calculations was continued until changes in the total energy become less than 10^{-8} Hartree. When performed, the crystal structure was optimized completely (both the unit cell parameters and atomic positions) until simultaneously four thresholds were reached: the largest absolute (la) and root-mean-square (rms) values of atomic forces became smaller than 4.5×10^{-4} a.u. and 3.0×10^{-4} a.u. and the la and rms values of atomic displacements became smaller than 1.8×10^{-3} a.u. and 1.2×10^{-3} a.u., respectively. The Stuttgart/Cologne group effective core potentials[27] (ECP) were used for Bi and the all-electron approach for Fe and O atoms. The basis set optimization and details of the thermodynamic analysis of BFO stability will be described in detail in an upcoming paper.[28]

At ambient conditions, BFO has the same ferroelectric (FE) perovskite structure as common ferroelectric $LiNbO_3$ ($R3c$, #161 symmetry space group). The calculations of BFO in the FE atomic configuration were performed with the unit cell corresponding to the rhombohedral symmetry with two formula units. The cubic centro-symmetric perovskite configuration of BFO was modeled by unit cells containing 8 formula units ($2 \times 2 \times 2$ extended unit cell with respect to a minimal perovskite unit cell of 5 atoms), in order to include into the modeling all possible anti-ferromagnetic (AFM) magnetic orders. There are three possible AFM orders for the perovskite lattice: (i) in the A-type AFM the Fe spins have ferromagnetic ordering within (001) planes, but spins in the nearest neighboring planes have opposite orientations; (ii) in the C-type AFM order, spins are ferromagnetically ordered along one of the [001] directions, but AFM-ordered in the planes perpendicular to this direction; (iii) in the G-type AFM order, all nearest-neighboring iron atoms have opposite directions of their spins. In the cubic perovskite structure, FM and all possible AFM orders were modeled. For the FE structure of BFO only FM and one AFM spin orders were considered; the AFM configuration coincides with the G-type AFM spin order.

The main results are presented in Table 1. In agreement with experiments, the G-type AFM spin order is the most stable configuration for both FE and cubic BFO. The structure of the FE state lowest in energy with the AFM (G) spin order is very well reproduced in the present calculations as well: the largest deviation in the calculated vs experimental lattice parameters is 0.9%. The cubic structure is by ~1 eV higher than the FE one. The FM state is the highest in energy. The AFM C-type state is lower in total energy than the A-type state. The calculated and experimental atomic positions within the FE unit cell of BFO

DOI: 10.1021/acs.jpclett.5b01071
J. Phys. Chem. Lett. 2015, 6, 2847−2851

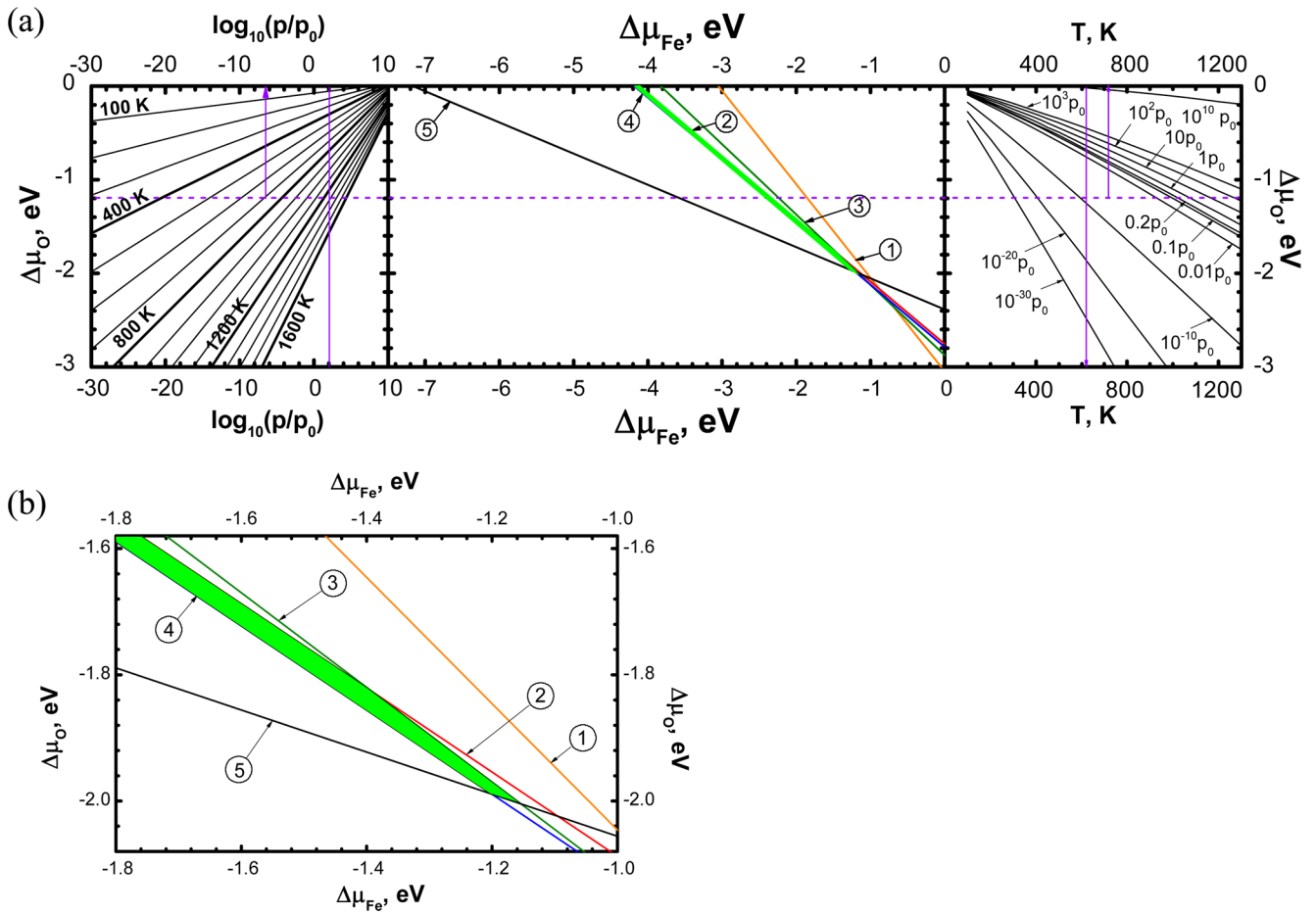

Figure 1. (a) Phase diagrams for $BiFeO_3$ based on hybrid density functional calculations with all electrons on Fe ions included explicitly. The formation energies used to build these diagrams are provided in Table 3. The numbered lines in the central panel describe conditions of forming of (1) FeO; (2) Fe_2O_3; (3) Fe_3O_4; (4) Bi_2O_3; (5) Bi metal. Green area marks the region of $BiFeO_3$ stability. Side panels serve to convert values of oxygen chemical potential to easily observable values of temperature T and oxygen partial pressure p_{O_2}. (b) Enlargement of the region marked by a rectangular from panel a. See the text and refs 28 and 36−39 for more details on applied technique. The variation of chemical potential for Fe atoms is defined as the deviation of Fe atoms chemical potential from its value in metallic iron ($\Delta\mu_{Fe} \approx \mu_{Fe} - E_{Fe}$), which is the standard state for the iron and approximated by the total energy of Fe atom in Fe metal. Similarly, the variation of O atom chemical potential is calculated with respect to the total energy of O atom in O_2 molecule ($\Delta\mu_O = \mu_O - (1/2)\, E_{O_2}$).

are compared in Table 2. The optimized atomic coordinates are again in very good agreement with experimental results.[29]

The calculated formation energies and standard formation Gibbs energies for binary oxides are presented in Table 3; these were used to draw the phase diagrams necessary for the analysis of BFO stability. The temperature dependence of the Gibbs energies of formation is determined here only by the chemical potential of O_2 gas, i.e., vibrational contributions in the solid phases are neglected. The experimental data on O_2 gas were taken from NIST Chemistry WebBook.[30] The energies of formation were calculated using the ab initio total energies for the elemental materials; the standard Gibbs energies of formation account for change in the Gibbs energy of O_2 gas between $T = 0$ K and standard conditions ($T = 298.15$ K). The calculated Gibbs energies of formation for iron oxides allow us to estimate the quality of the employed hybrid functional and the procedure for calculating the formation energies. The largest deviation of the calculated from the experimental standard formation Gibbs energy is for FeO (5.9% for calculations with ECP and 7.6% for all-electron calculations). At the same time, the absolute deviation of the calculated standard formation Gibbs energy is even smaller than for Fe_3O_4. This is because the Gibbs energy of formation for FeO is approximately a factor of 3 smaller than that for Fe_3O_4. Ultimately, the accumulation of error resulted in noticeable deviations in the formation Gibbs energy for BFO (~10%).

The formation energies and the formation Gibbs energies for BFO from Bi_2O_3 and Fe_2O_3 are only −0.05 eV/f.u., being considerably underestimated as compared to the formation enthalpies calculated from experimental data.[31,32] However, these formation Gibbs energies still have the correct sign, corresponding to weakly stable BFO with respect to decomposition into Bi and Fe binary oxides. The formation energies are important because they determine the width of the stability region in the phase diagram (Figure 1). A similar estimate was done previously with LDA+U method and plane wave basis set yielding the BFO formation energy from the binary oxides[14] equal to −0.2 eV. This value is more negative than that obtained in our calculations, but it still is much smaller compared with the experimental results. The deviation in the calculated formation energy for BFO from the oxides can arise due to shortcomings of the B3PW hybrid density functional and due to neglect of the vibrational contributions

DOI: 10.1021/acs.jpclett.5b01071
J. Phys. Chem. Lett. 2015, 6, 2847−2851

of solids to the formation energies. Both possibilities have to be tested in the future.

We limited our consideration to a study of BFO stability with respect to simple oxides and reduction of the metals. However, it was found experimentally that BFO becomes unstable in the temperature interval 720−1040 K with respect to decomposition[32−35] to complex ternary oxides $Bi_{25}FeO_{39}$ and $Bi_2Fe_4O_9$. These materials have large size of unit cells and noncollinear spin ordering. Therefore, theoretical modeling of such materials is much more difficult and demands large computational time and resources, preventing us from including such a study at the present time.

The calculated BFO formation energies (Table 3) were used to build the phase diagrams presented in Figure 1 (see refs 28 and 36−39 for more details on building such phase diagrams). The complete diagram in Figure 1a contains 3 panels. The phase diagram is plotted in the central panel. The numbered lines represent conditions for precipitation of Bi metal, Bi and Fe oxides, and BFO, whereas the green area represents the region of BFO stability. The employed theory assumes that within the stability regions the stoichiometric ratio of metals is strictly preserved or, in other words, the number of Bi and Fe atoms must be equal and the formation of defects is not allowed. Under this condition, the external environment (temperature and partial pressure of oxygen gas) determines only the sum of the chemical potentials of the metals. The chemical potentials of the involved metals could be determined separately, if at least one other material is present in the system.

The two side panels in the phase diagrams in Figure 1a serve for a conversion of the chemical potential of the oxygen atom to the observables (temperature and oxygen gas partial pressure). On the right panel, it is presented as a function of temperature for a set of preselected oxygen gas pressures. On the left panel, the O atom chemical potential is presented as a function of pressure for a considered range of temperatures (the increment between neighboring lines is 100 K).

These panels can be used in two ways. One can draw vertical lines on the panels for a selected temperature (at the right panel) or pressure (at the left panel). This is illustrated by vertical lines at side panels in Figure 1a. Crossings between these lines and functions plotted at the panels produce scales to measure pressure (temperature) for the selected temperature (pressure) at the right (left) panel, correspondingly. Alternatively, one might want to determine temperature (pressure) at a specific pressure (temperature) for a point in the phase diagram. For this purpose, a horizontal line can be drawn through this point; then the desired temperature (pressure) can be found at the crossing of this horizontal line with the line for desirable pressure (temperature) at the right (left) panel. This approach is illustrated in Figure 1a by a dotted horizontal line and vertical arrows.

The BFO stability region is restricted by Bi_2O_3, Bi metal, Fe_2O_3, and Fe_3O_4 precipitation lines for the phase diagram built using calculations with the all-electron description of the Fe atoms. This qualitatively coincides with the phase diagram based on experimental data discussed in ref 28; however, the phase diagram presented in Figure 1 is much narrower than the one built from experimental formation energies. The diagram in Figure 1 predicts that BFO decomposes into Fe_3O_4, metallic Bi and O_2 gas ($3BiFeO_3 \rightarrow Fe_3O_4 + 3\ Bi + O_2$) when the ratio of Bi and Fe atoms in the system is maintained, while the chemical potential of the O atom decreases enough. The latter corresponds to increase of temperature and/or decrease of O_2 partial pressure. In both these cases, if there is an excess of Fe atoms, Fe_2O_3 reduces to Fe_3O_4 before the chemical potential of O atoms reaches the value of BFO decomposition. It is easier to see all described transformations on Figure 1b, where enlargement of the phase diagram at low values of O atom chemical potential is provided.

In summary, the atomic structure of multiferroic BFO was calculated using the B3PW hybrid density functional. In the first approximation, the vibrational contribution into the Gibbs energy of solid compounds was neglected, and the temperature dependence of the Gibbs energies of formation arises entirely due to change in the Gibbs energy for oxygen gas. The obtained results are in good agreement with experiments. The performed ab initio calculations allow us to obtain all necessary Gibbs energies of formation for the considered compounds, in order to build phase diagrams and analyze the decomposition products that determine the boundaries of the stability region of BFO and can coexist with it. The same kind of diagram could be built using the experimental Gibbs energies of formation.[28] All these diagrams allow understanding of possible chemical transformations in the system, whenever the system contains equal number of Fe and Bi atoms or there is an excess of Fe or Bi. The calculated crystal structures and formation energies are very close and reproduce reasonably well-known experimental data for iron oxides. Note that the variation range of the chemical potential of the O atom, within which BFO is stable, could also be determined from the phase diagrams and then drawn on a contour map for the chemical potential of the O atom.[28]

We have developed here a novel methodology for the analysis of advanced material stability in terms of external parameters: temperature and partial gas pressure. The present advanced hybrid calculations show a surprising underestimate of the BFO formation energy at 0 K, similar to the previous standard LDA calculations. This leads to a very narrow area of BFO stability, which is defined here by the formation energy of BFO from Bi_2O_3 and Fe_2O_3. This could result from deficiency of the employed B3PW functional. Therefore, further testing of available hybrid functionals is needed.

AUTHOR INFORMATION

Corresponding Authors

*E-mail: e.kotomin@fkf.mpg.de (E.A.K.).
*E-mail: eheif5719@sbcglobal.net (E.H.).

Notes

The authors declare no competing financial interest.

ACKNOWLEDGMENTS

Authors are indebted to R. Merkle for many fruitful discussions. This research was partly funded by the EC GREEN-CC FP7 project 608524, and computer resources partly were provided by Juelich Supercomputing Center (Project HSS15). E.H. thanks Department of Physical Chemistry of the Max Planck Institute for Solid State Research for long-term hospitality and support. E.H., E.A.K., and A.A.B. acknowledge the Russian Science Foundation for provided financial support for the analysis of the experimental literature on complex perovskite formation enthalpy through funding under the project 14-43-00052.

DOI: 10.1021/acs.jpclett.5b01071
J. Phys. Chem. Lett. 2015, 6, 2847−2851

REFERENCES

(1) Catalan, G.; Scott, J. F. Physics and Applications of Bismuth Ferrite. *Adv. Mater.* **2009**, *21*, 2463−2485.

(2) Batzill, M. Fundamental Aspects of Surface Engineering of Transition Metal Oxide Photocatalysts. *Energy Environ. Sci.* **2011**, *4*, 3275−3286.

(3) Yang, S. Y.; Martin, L. W.; Byrnes, S. J.; Conry, T. E.; Basu, S. R.; Paran, D.; Reichertz, L.; Ihlefeld, J.; Adamo, C.; Melville, A.; et al. Photovoltaic Effects in $BiFeO_3$. *Appl. Phys. Lett.* **2009**, *95*, 062909.

(4) Wedig, A.; Merkle, R.; Stuhlhofer, B.; Habermeier, H.-U.; Maier, J.; Heifets, E. Fast Oxygen Exchange Kinetics of Pore-Free $Bi_{1-x}Sr_xFeO_3- \delta$ Thin Films. *Phys. Chem. Chem. Phys.* **2011**, *13*, 16530−16533.

(5) Wedig, A.; Lynch, M. E.; Merkle, R.; Maier, J.; Liu, M. Sheet Resistance in Thin Film Solid Oxide Fuel Cell Model Cathodes: A Case Study on Circular $Bi_{1-x}Sr_xFeO_{3-\delta}$ Microelectrodes. *ECS Trans.* **2012**, *45*, 213−224.

(6) Wedig, A.; Merkle, R.; Maier, J. Oxygen Exchange Kinetics of (Bi, Sr)(Co, Fe) $O_{3-\delta}$ Thin-Film Microelectrodes. *J. Electrochem. Soc.* **2014**, *161*, F23−F32.

(7) Li, S. W.; You, C.; Fang, L. Q.; Yang, W. S.; Lin, L. W.; Meng, J. A.; Ren, Y. F. Oxygen Permeating Properties of the Mixed Conducting Membranes without Cobalt. *Mater. Res. Bull.* **1998**, *33*, 183−188.

(8) Shao, Z. P.; Cong, Y.; Xiong, G. X.; Sheng, S. S.; Yang, W. S. Mixed-Conducting Perovskite-Type $Sr_xBi_{1-x}FeO_{3-\delta}$ Oxygen-Permeating Membranes. *Sci. China, Ser. B: Chem.* **2000**, *43*, 421−427.

(9) Brinkman, K.; Iijima, T.; Takamura, H. The Oxygen Permeation Characteristics of $Bi_{1-x}Sr_xFeO_3$ Mixed Ionic and Electronic Conducting Ceramics. *Solid State Ionics* **2010**, *181*, 53−58.

(10) Niu, Y. J.; Zhou, W.; Sunarso, J.; Ge, L.; Zhu, Z. H.; Shao, Z. P. High Performance Cobalt-Free Perovskite Cathode for Intermediate Temperature Solid Oxide Fuel Cells. *J. Mater. Chem.* **2010**, *20*, 9619−9622.

(11) Niu, Y. J.; Sunarso, J.; Zhou, W.; Liang, F. L.; Ge, L.; Zhu, Z. H.; Shao, Z. P. Evaluation and Optimization of $Bi_{1-x}Sr_xFeO_{3-\delta}$ Perovskites as Cathodes of Solid Oxide Fuel Cells. *Int. J. Hydrogen Energy* **2011**, *36*, 3179−3186.

(12) Niu, Y. J.; Sunarso, J.; Liang, F. L.; Zhou, W.; Zhu, Z. H.; Shao, Z. P. A Comparative Study of Oxygen Reduction Reaction on Bi- and La-doped $SrFeO_{3-\delta}$ Perovskite Cathodes. *J. Electrochem. Soc.* **2011**, *158*, B132−B138.

(13) Baek, D.; Kamegawa, A.; Takamura, H. Preparation and Electrode Properties of Composite Cathodes Based on $Bi_{1-x}Sr_xFeO_{3-\delta}$ with Perovskite-Type Structure. *Solid State Ionics* **2014**, *262*, 691−695.

(14) Zhang, Z.; Wu, P.; Chen, L.; Wang, J. Density Functional Theory Plus U Study of Vacancy Formations In Bismuth Ferrite. *Appl. Phys. Lett.* **2010**, *96*, 232906.

(15) Paudel, T. R.; Jaswal, S. S.; Tsymbal, E. Y. Intrinsic Defects in Multiferroic $BiFeO_3$ and Their Effect on Magnetism. *Phys. Rev. B: Condens. Matter Mater. Phys.* **2012**, *85*, 104409.

(16) Mei, Zh.-G.; Shang, Sh.; Wang, Y.; Liu, Z.-K. Thermodynamics of Multiferroic: Applications for the Deposition of Thin Films. *Appl. Phys. Lett.* **2011**, *98*, 131904.

(17) Franchini, C. Hybrid Functionals Applied to Perovskites. *J. Phys.: Condens. Matter* **2014**, *26*, 253202.

(18) Alkauskas, A.; Deak, P.; Neugebauer, J.; Pasquarello, A.; Van de Walle, C. G., Eds.; *Advanced Calculations for Defects in Materials: Electronic Structure Methods*; John Wiley & Sons: Hoboken, NJ, 2011.

(19) Evarestov, R. A. *Quantum Chemistry of Solids*; Series in Solid State Sciences; Springer: New York, 2014; Vol. *153*.

(20) Dovesi, R.; Saunders, V. R.; Roetti, C.; Orlando, R.; Zicovich-Wilson, C. M.; Pascale, F.; Civalleri, B.; Doll, K.; Harrison, N. M.; Bush, I. J.; et al. *CRYSTAL09 User's Manual*; University of Torino: Torino, Italy, 2009. http://www.crystal.unito.it/Manuals/crystal09.pdf.

(21) Becke, D. Density-Functional Thermochemistry. III. The Role of Exact Exchange. *J. Chem. Phys.* **1993**, *98*, 5648−5652.

(22) Perdew, J. P.; Wang, Y. Accurate and Simple Density Functional for the Electronic Exchange Energy: Generalized Gradient Approximation. *Phys. Rev. B: Condens. Matter Mater. Phys.* **1986**, *33*, 8800−8802.

(23) Perdew, J. P.; Wang, Y. Erratum: Accurate and Simple Density Functional for the Electronic Exchange Energy: Generalized Gradient Approximation. *Phys. Rev. B: Condens. Matter Mater. Phys.* **1989**, *40*, 3399−3399.

(24) Perdew, J. P.; Wang, Y. Accurate and Simple Analytic Representation of the Electron-Gas Correlation Energy. *Phys. Rev. B: Condens. Matter Mater. Phys.* **1992**, *45*, 13244−13249.

(25) Perdew, J. P. *Electronic Structure of Solids*; Akademie Verlag: Berlin, 1991.

(26) Parameters of TOLINTEG keywords were set to 8 8 8 8 16. These parameters determine the thresholds controlling the level of approximation in calculations of different Coulomb and exchange integrals. See CRYSTAL User's Manual[5] for more details.

(27) Stuttgart/Cologne energy-consistent (ab initio) pseudopotentials suitable for wavefunction-based and density functional calculations. http://www.tc.uni-koeln.de/PP/index.en.html.

(28) Heifets, E.; Kotomin, E. A.; Maier, J. (in preparation).

(29) Sosnowska, I.; Schäfer, W.; Kockelmann, W.; Andersen, K. H.; Troyanchuk, I. O. Crystal Structure And Spiral Magnetic Ordering of $BiFeO_3$ Doped with Manganese. *Appl. Phys. A: Mater. Sci. Process.* **2002**, *74*, S1040−S1042.

(30) Linstrom, P. J.; Mallard, W. G., Eds.; *NIST Chemistry WebBook, NIST Standard Reference Database No. 69*; National Institute of Standards and Technology: Gaithersburg, MD, 2003. http://webbook.nist.gov/chemistry/.

(31) *Scientific Group Thermodata Europe in Thermodynamic Properties of Inorganic Materials, Landolt-Börnstein, New Series*, Group IV Vol. *19*; edited by Lehrstuhl für Theoretische Hüttenkunde; Springer: Berlin, 1999.

(32) Phapale, S.; Mishra, R.; Das, D. Standard Enthalpy of Formation and Heat Capacity of Compounds in the Pseudo-Binary Bi_2O_3−Fe_2O_3 System. *J. Nucl. Mater.* **2008**, *373*, 137−141.

(33) Carvalho, T. T.; Tavares, P. B. Synthesis and Thermodynamic Stability of Multiferroic $BiFeO_3$. *Mater. Lett.* **2008**, *62*, 3984−3986.

(34) Selbach, S. V.; Einarsrud, M.-A.; Grande, T. On the Thermodynamic Stability of $BiFeO_3$. *Chem. Mater.* **2009**, *21*, 169−173.

(35) Lu, J.; Qiao, L. J.; Fu, P. Z.; Wu, Y.C. J. Phase Equilibrium of Bi_2O_3−Fe_2O_3 Pseudo-Binary System and Growth of $BiFeO_3$ Single Crystal. *J. Cryst. Growth* **2011**, *318*, 936−941.

(36) Heifets, E.; Kotomin, E. A.; Mastrikov, Yu. A.; Piskunov, S.; Maier, J. Thermodynamics of ABO_3-type Perovskite Surfaces. In *Thermodynamics - Interaction Studies - Solids, Liquids and Gases*, edited by Moreno, J. C.; InTech: Rijeka, Croatia, 2011. http://www.intechopen.com/articles/show/title/thermodynamics-of-abo3-type-perovskite-surfaces.

(37) Heifets, E.; Piskunov, S.; Kotomin, E. A.; Zhukovskii, Yu. F.; Ellis, D. E. Electronic Structure and Thermodynamic Stability of Double-Layered $SrTiO_3$(001) Surfaces: *Ab Initio* Simulations. *Phys. Rev. B: Condens. Matter Mater. Phys.* **2007**, *75*, 115417.

(38) Heifets, E.; Ho, J.; Merinov, B. Ab Initio Simulation of the $BaZrO_3$ (011) Surface Structure. *Phys. Rev. B: Condens. Matter Mater. Phys.* **2007**, *75*, 155431.

(39) Ahmad, E. A.; Liborio, L.; Kramer, D.; Mallia, G.; Kucernak, A. R.; Harrison, N. M. Thermodynamic Stability of LaMnO3 and Its Competing Oxides: A Hybrid Density Functional Study of an Alkaline Fuel Cell Catalyst. *Phys. Rev. B: Condens. Matter Mater. Phys.* **2011**, *84*, 085137.

DOI: 10.1021/acs.jpclett.5b01071
J. Phys. Chem. Lett. 2015, 6, 2847−2851